Int. J. Multiphase Flow. Vol. 4. pp. 157–170. Pergamon/Elsevier. 1978. Printed in Great Britain

BEHAVIOUR OF LIQUID FILMS AND FLOODING IN COUNTER-CURRENT TWO-PHASE FLOW. PART 2. FLOW IN ANNULI AND ROD BUNDLES

T. UEDA and S. SUZUKI*

Department of Mechanical Engineering, University of Tokyo, Bunkyo-ku, Tokyo 113, Japan

(*Received* 7 *September* 1977)

Abstract—Experiments are described on the gas velocity at the onset of flooding and the maximum height of the wavy liquid film flowing downwards on a rod surface. On the basis of a simple analysis for a large amplitude wave on the liquid film, a flooding condition relating the maximum wave height to the gas velocity at the onset of flooding is derived. The values predicted by this condition show a good agreement with the measured results.

An equivalent diameter of the channel is defined for the flooding velocity. Applying this diameter, the present data for annuli and rod bundles are well correlated by the same empirical equation as that for flow in circular tubes presented previously.

1. INTRODUCTION

The flooding phenomenon is closely connected with the wave instability due to interaction between the liquid surface waves and the upward gas stream. Therefore, the flooding velocity, i.e. the gas velocity at the onset of flooding is, as mentioned in the paper Part 1 (Suzuki & Ueda 1977) is strongly affected by the cross-sectional area of the flow channel. In the cases where the liquid films flow down on the outer surface of vertical tubes and the gas flows the outside, the channel cross-sections are usually complicated. The flooding in such cross-sections as rod bundles has become of wide interest in connection with the safety of light water reactors. However, study on these cases (Shires & Pickering 1965; Shires *et al.* 1964) is limited comparing with that of flow in circular tubes.

In this report, the flooding phenomenon is investigated on the flow in annuli. Experimental results are presented on the flooding velocity and the maximum height of the liquid film measured by a contact probe method. A simple analysis for a large amplitude wave on the liquid film is proposed and discussions are presented on the flooding condition. Measurements of the flooding velocity are also made on bundles of three and four rods with various channel cross-sections, and the results are correlated in terms of nondimensional groups by using an equivalent diameter.

2. EXPERIMENTAL APPARATUS AND PROCEDURE

Figure 1 shows a schematic diagram of the experimental apparatus and figure 2 the cross-sections of the test channel. The test channel consists of stainless steel pipes simulating the rods of a fuel element and a shroud pipe made of transparent acrylic resin. The dimensions of the stainless pipes are 10 mm in outside diameter and 1.0 m in length.

The air introduced from a bell-shaped section flows through the test channel and an upper tube, and is delivered to the atmosphere by a turbo-blower. On the other hand, the liquid pumped up from a tank is supplied in the sintered bronze sections of 10 mm O.D., 5 mm I.D. and 80 mm long fitted on the top of each rod. The liquid passed through the sinter sections from the inside to outside flows down on the surface of the rods in a state of films. When the air flow rate is below the flooding point, all the liquid flows downwards and falls from the bell-shaped section to a drain receiver. However, when the air flow rate is above the flooding point, part of the liquid flows upwards accompanied with the gas stream and is separated at a connecting box and a drain separator. In this experiment, the liquid temperature at the storage tank was kept in a range of 25 ± 1 °C.

*Present address: Unicellex Development Division, Unitika Ltd., Uji-City, Kyoto 611, Japan.

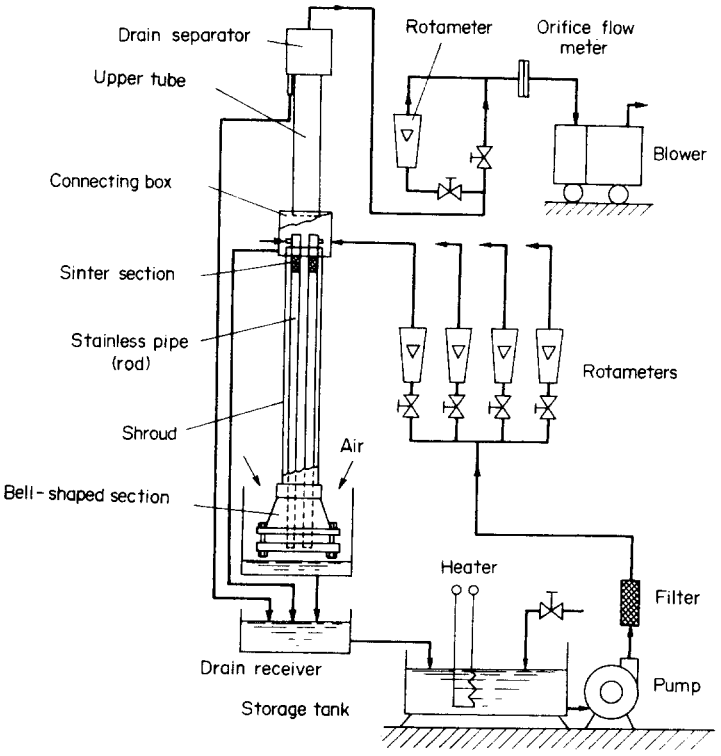

Figure 1. Schematic diagram of experimental apparatus.

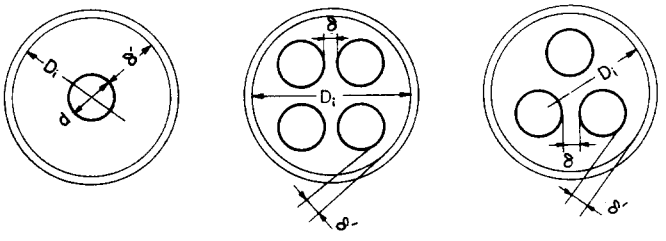

Figure 2. Cross-sections of test channel.

Table 1. Dimensions of test channel

Annulus	(mm)		
Rod–shroud δ'	9.0	12.5	15.0
Shroud diameter D_i	28	35	40

Rod diameter
d = 10.0 mm

Rod length
L_d = 1.0 m

Bundle of three rods

Dimensions (mm)	$\delta = \delta'$			$\delta = 4.2$			$\delta' = 4.2$		
Rod–rod δ	2.0	4.2	5.9	4.2	4.2	4.2	4.2	6.9	8.7
Rod–shroud δ'	2.0	4.2	5.9	2.7	4.2	6.7	4.2	4.2	4.2
Shroud diameter D_i	28	35	40	32	35	40	35	38	40

Bundle of four rods

Dimensions (*mm*)	$\delta = \delta'$			$\delta = 4.1$			$\delta' = 4.1$		
Rod–rod δ	2.3	4.1	6.1	4.1	4.1	4.1	4.1	5.4	9.0
Rod–shroud δ'	2.3	4.1	6.1	2.5	4.1	7.5	4.1	4.1	4.1
Shroud diameter D_i	32	38	45	35	38	45	38	40	45

The flooding velocity was determined by increasing gas flow rate in a small increment under a constant liquid flow rate. For the purpose of examining the effect of the cross-sectional area of the flow channel on flooding, the dimensions of the test channel were varied systematically as is shown in table 1. The experiment was carried out in a range of liquid flow rates per rod Q_L = 0.2–1.0 l/min and liquid film Reynolds numbers $Re_L = 4\rho_L Q_L/(\mu_L \pi d)$ = 472–2360.

The maximum height of the liquid film was measured by the same method as that described in the previous paper. The measurements were made at the positions 0.3, 0.6 and 0.9 m downstream of the sinter section. The upward air velocity distribution across the test channel was also investigated by a fine pitot tube and a Chattock type micromanometer. Since the pitot tube was frequently clogged up by water droplets in counter-current two-phase flow, this measurement was made on single-phase air flow.

The waves on the liquid film grow up as the gas flow rate is increased. If the gas flow rate is further increased progressively, droplets are generated from some of the waves and attach on the inner surface of the shroud, and then a point is reached at which a large amplitude wave is formed on the liquid film. This wave extends as if it covered most of the channel cross-section, and is immediately carried upwards by the gas stream. An example of the experimental results is shown in figure 3. In many cases of rod bundles, there was some difference in the gas velocity between the initial flooding, i.e. the initial formation of the extended wave carried upwards and the continuous formation of the extended wave. However, the difference in the gas velocity was relatively small, then, the flooding velocity is defined in this paper as the gas velocity at the initial formation of the extended wave. When the gas velocity is above the flooding point, part of the liquid flows upwards and the remainder falls down along the rod surface and the shroud wall.

3. EXPERIMENTS ON FLOW IN ANNULI

The experimental results of the flooding velocity u_G are shown in figure 4 versus the liquid volume flow rate Q_L and the mean liquid film thickness y_i. Here the value u_G is the gas velocity at the onset of flooding and y_i is the value determined for Q_L by means of the relationship between the nondimensional mean film thickness and film Reynolds number as mentioned in the previous paper. The flooding velocity shows a trend to decrease with an increase of the liquid flow rate and takes higher values with an increase of the inside diameter of the shroud.

Figures 5 and 6 show the experimental results of the maximum height of the liquid film y_{imax} obtained in an annulus with a rod of diameter d = 10 mm and a shroud of inside diameter D_i = 40 mm. Figure 5 represents the variations of the maximum height of the liquid film along the rod in the absence of upward gas stream. In this experimental range of low liquid film Reynolds numbers, the effect of surface tension was remarkable. The data for an aqueous

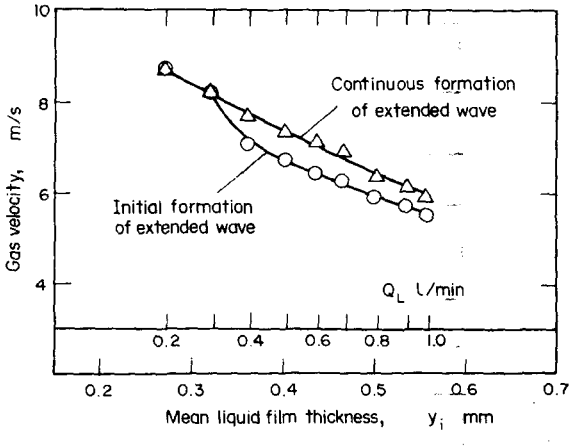

Figure 3. Formation of extended wave carried upwards. (Air–water flow in a bundle of four rods; δ = 4.1 mm, δ' = 2.5 mm, D_i = 35 mm)

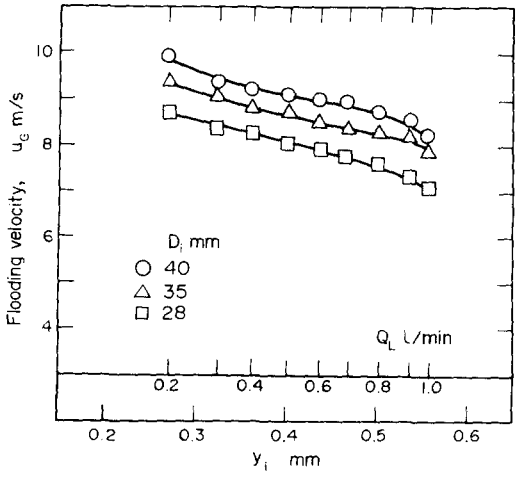

Figure 4. Flooding velocity for air–water flow in annuli.

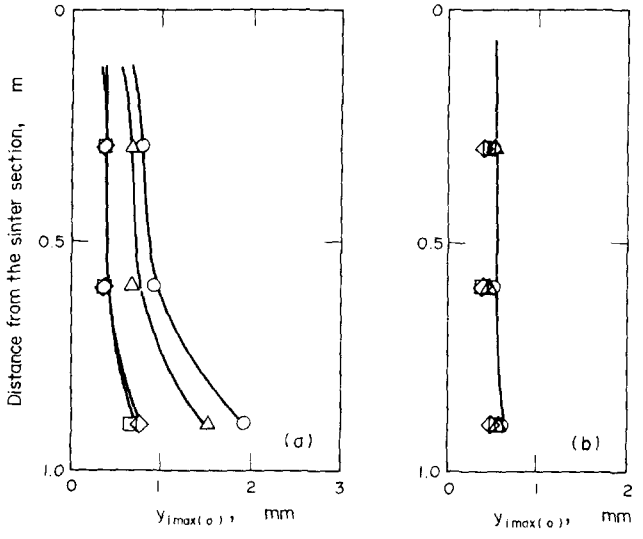

Figure 5. Maximum height of falling liquid film. (Annulus; $d = 10$ mm, $D_i = 40$ mm, $u = 0$ m/s) (a) Water films, $\sigma = 0.068$ N/m (b) Aqueous sec.-octyl alcohol solution films, $\sigma = 0.045$ N/m.

	Re_L	y_i mm
○	2120	0.53
△	1650	0.47
□	1180	0.40
◇	708	0.32

alcohol solution of low surface tension $\sigma = 4.5 \times 10^{-2}$N/m show that the maximum heights of the liquid films are close to the mean film thicknesses y_i—figure 5, (b). Figure 6 shows the measured maximum height of the water film at a position $L = 0.9$ m plotted versus the gas velocity. In a range of high gas velocities, the wave height increases steeply with increasing gas velocity and reaches the flooding point. The solid points in the figure are the values of y_{imax} just before the flooding. The dotted line represents a relation between the maximum height of the liquid film and the gas velocity at the flooding condition. As for liquid films of the aqueous alcohol solution, it was difficult to measure the maximum height of the film just before flooding because droplet entrainment was intensive near the flooding point.

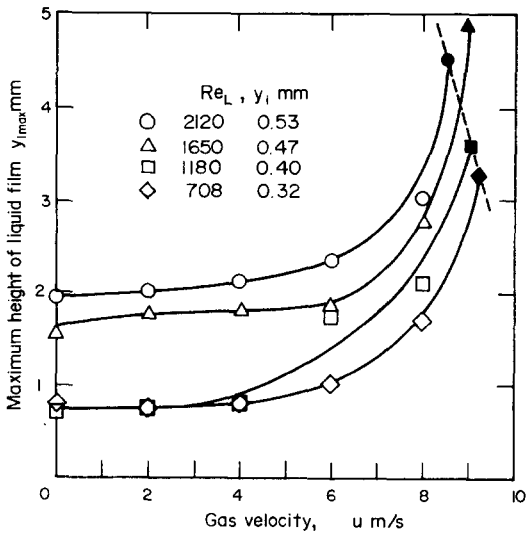

Figure 6. Maximum height of liquid film and gas velocity. (Air–water flow in an annulus; D_i = 40 mm, Probe position L = 0.90 m).

4. MECHANISM OF FLOODING

4.1 *Analysis*

Some theoretical studies have been made on the mechanism of flooding. A unique theory was constructed by Shearer & Davidson (1965) on a standing wave which was formed by the action of counter-current air flow on the liquid film flowing downwards on a rod placed in the center of an orifice. According to their theory, the amplitude of the standing wave has a trend to grow abruptly large at a critical air velocity. Thus, it is supposed that flooding phenomenon is associated with the wave instability. Assuming the existence of infinitesimal sinusoidal waves at the liquid–gas interface, Getinbudakler & Jameson (1969) applied the famous Orr–Sommerfeld equation derived from the Navier Stokes equation to laminar liquid films. This equation was combined with the boundary conditions obtained by taking into account the effect of gas stream on the interface, and finally the critical gas velocity required to cause unstable waves was calculated with the aid of the numerical technique. Recently, Kusuda & Imura (1974) applied the instability theory for a simple system consisting of inviscid fluids to the counter-current two-phase flow, and derived the critical velocity between the gas and liquid phases at which interfacial waves became unstable.

In these theoretical studies, the mechanism of flooding is postulated as a phenomenon associated with the so-called wave instability. However, these theories give no suitable description on the effect of the cross-sectional area of the flow channel which has actually a remarkable influence on the flooding velocity. It has been observed that the large wave formed on the liquid film is carried upwards by the gas stream at the flooding point, but this fact is not considered in the above theories. Moreover, Getinbudakler & Jameson (1969) and Kusuda & Imura (1974) assumed sinusoidal waves on the liquid film. However, since the maximum height of the liquid film is usually several times as large as the mean film thickness, there are some questions on the wave model.

In the previous paper, it has been shown that the effects of some factors on flooding can be explained qualitatively by taking into account the characteristics of the maximum height of the liquid film and that there is a relation between the maximum height of the liquid film and the gas velocity at the flooding point. Then, based on a simplified model of the interfacial wave, an analysis is proposed here for interaction between the large amplitude wave on the liquid film and the upward gas stream at the onset of flooding.

According to the observation, flooding takes place when a large amplitude wave is formed

on the liquid film and carried upwards by the gas stream. At this condition, it is expected that part of the liquid is continuously torn off from the crest of the large amplitude wave and breaks up into droplets. As is well known, the liquid film is wavy and the pressure of the gas phase flowing on the wave crest is reduced due to the resultant acceleration of the gas flow. If the gas velocity is increased, the gas pressure on the crest decreases further because the wave amplitude becomes large with increasing gas velocity. In the range of low gas velocities, the wave on the liquid film is stable due to the surface tension acting on the wave surface. However, when the gas velocity is raised above a critical value, the pressure difference caused on the wave crest overcomes the surface tension. Therefore, flooding is thought to be connected with this force balance.

As a possible model, consider a state at the critical condition mentioned above. Figure 7 illustrates a liquid lump of a single large amplitude wave formed on the steady liquid film. Shape of the wave crest is assumed to be flat because the wave tip is continuously torn off by the gas stream. In this analysis the following assumptions are used;

(1) Location of the liquid lump is fixed in space.

(2) Shear stresses on the gas–liquid interface and the shroud surface are negligible excepting those on the liquid lump.

(3) Both gravity force and compressibility of the gas phase are negligible.

Here, the force balances on the liquid lump is set up in both horizontal and vertical directions. In figure 7, Δh and δ_w denote the height and width of the lump of large wave, p the pressure and A_G and A_L, u_G and u_L, and ρ_G and ρ_L are the cross-sectional areas, mean velocities and densities of the gas and liquid phases, respectively.

First, consider the variation of the gas phase pressure along the channel. The pressure loss Δp between the sections 1 and 2 can be expressed approximately as the sum of an abrupt contraction loss Δp_ζ and an abrupt expansion loss Δp_ξ at the section 0.

$$\Delta p = \Delta p_\zeta + \Delta p_\xi. \qquad [1]$$

The abrupt contraction loss is given by

$$\Delta p_\zeta = \zeta_0 \frac{\rho_G}{2} u_{G0}^2 = \zeta_1 \frac{\rho_G}{2} u_{G1}^2 \qquad [2]$$

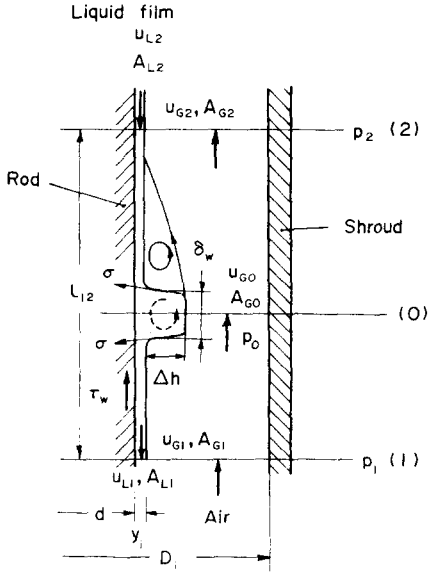

Figure 7. Analytical model.

where the loss coefficient ζ_0 is a function of the ratio of A_{G0} to A_{G1}. The loss coefficient ζ_1 defined for the gas velocity u_{G1} can be obtained from the value of ζ_0 and the continuity equation $u_{G0}A_{G0} = u_{G1}A_{G1}$. In the range of $(A_{G0}/A_{G1}) = 0.4 \sim 0.85$ in this experiment, ζ_1 can be approximated by the following equation,

$$\zeta_1 = (A_{G1}/A_{G0}) - 1.$$

Therefore,

$$\Delta p_\zeta = \left[\left(\frac{A_{G1}}{A_{G0}}\right) - 1\right]\frac{\rho_G}{2}u_{G1}^2. \qquad [3]$$

The abrupt expansion loss Δp_ξ is usually given by the following equation,

$$\Delta p_\xi = \xi\frac{\rho_G}{2}(u_{G0} - u_{G2})^2 \qquad [4]$$

where the value of the loss coefficient ξ can be approximated as unity. Since the thickness of the liquid film y_i is uniform along the rod excepting the part of the liquid lump, then $A_{G1} = A_{G2}$ and $u_{G1} = u_{G2}$. Therefore,

$$\Delta p_\xi = \left[\left(\frac{A_{G1}}{A_{G0}}\right) - 1\right]^2\frac{\rho_G}{2}u_{G1}^2. \qquad [5]$$

Combining [1], [3] and [5] gives

$$p_1 - p_2 = \Delta p = \frac{\rho_G}{2}u_{G1}^2\left(\frac{A_{G1}}{A_{G0}}\right)\left[\left(\frac{A_{G1}}{A_{G0}}\right) - 1\right]. \qquad [6]$$

Assuming that the gas phase pressure at each cross-section is uniform, the pressure loss between the sections 1 and 0 can be derived by applying Bernoulli's theorem,

$$p_1 - p_0 = \frac{\rho_G}{2}u_{G1}^2\left[\left(\frac{A_{G1}}{A_{G0}}\right)^2 - 1\right]. \qquad [7]$$

Next, let us consider the forces exerted on the liquid lump. At the critical condition, i.e. the onset of flooding, it is postulated that the force balances in both horizontal and vertical directions are realized on the liquid lump.

The force balance in the horizontal direction is

$$(p_1 - p_0)\delta_w = \eta_c\sigma \qquad [8]$$

where σ denotes the surface tension and η_c a factor depending on the wave profile. Although the pressure of liquid film varies from p_2 to p_1 between the sections 2 and 1, the pressure variation is relatively small. Then, the pressure in the liquid lump is assumed here to be equal to p_1. If the gas velocity is increased, the gas phase pressure p_0 is reduced further and the value of the L.H.S. in [8] becomes greater than that of $\eta_c\sigma$. Therefore, it appears to come into the flooding transition.

On the other hand, the equation of force balance in the vertical direction is derived by applying the momentum equation to the sections 1 and 2. The flow state is steady, $u_{L1} = u_{L2}$ for the liquid film and $u_{G1} = u_{G2}$ for the gas stream. Then,

$$p_1(A_{G1} + A_{L1}) = p_2(A_{G2} + A_{L2}) + \pi dl_{12}y_i\rho_L g + \pi(d + 2y_i)\delta_w\Delta h\rho_L g - \pi dl_{12}\tau_w$$

where d is the rod diameter and τ_w the shear stress on the rod surface. The shear stress on the interface is so small that $\tau_w \fallingdotseq y_i \rho_L g$, therefore

$$\pi(d + 2y_i)\delta_w \Delta h \rho_L g = (A_{G1} + A_{L1})\Delta p.$$

Taking into account $\pi(d + 2y_i)\Delta h = A_{G1} - A_{G0}$ and generally $A_{G1} \gg A_{L1}$, the above equation may be expressed as follows:

$$(A_{G1} - A_{G0})\delta_w \rho_L g = A_{G1}\Delta p. \qquad [9]$$

Then, from [6] and [9], the wave width at the onset of flooding is expressed as,

$$\delta_w = \frac{\rho_G}{\rho_L}\frac{u_{G1}^2}{2g}\left(\frac{A_{G1}}{A_{G0}}\right)^2. \qquad [10]$$

Therefore, substituting [7] and [10] into [8],

$$\left(\frac{\rho_G}{\rho_L}\frac{u_{G1}^2}{2g}\right)\left(\frac{\rho_G}{\sigma}\frac{u_{G1}^2}{2}\right)\left(\frac{A_{G1}}{A_{G0}}\right)^2\left[\left(\frac{A_{G1}}{A_{G0}}\right)^2 - 1\right] = \eta_c. \qquad [11]$$

This equation gives the relationship between the gas velocity u_{G1} and the wave height Δh at the onset of flooding because Δh is easily determined from (A_{G1}/A_{G0}). The profile factor is estimated as $\eta_c = 1.5$ by comparing the predicted values of [11] with the present experimental results of Δh–u_G for the annuli and also by referring the wave profile measured by Stainthorp & Batt (1965) in counter-current two-phase flow in a circular tube.

4.2 *Comparison with measured results*

In order to evaluate the validity of the above analysis, the analytical predictions are compared with the experimental data. The broken lines in figure 8 show the limit relationships calculated by [11] for air–water flow in the annuli of shroud diameters D_i, in which calculation the profile factor and the mean film thickness are assumed to be $\eta_c = 1.5$ and $y_i = 0.4$ mm, respectively. The data plotted in figure 8 are the wave height $\Delta h = y_{i\max} - y_i$ obtained from the

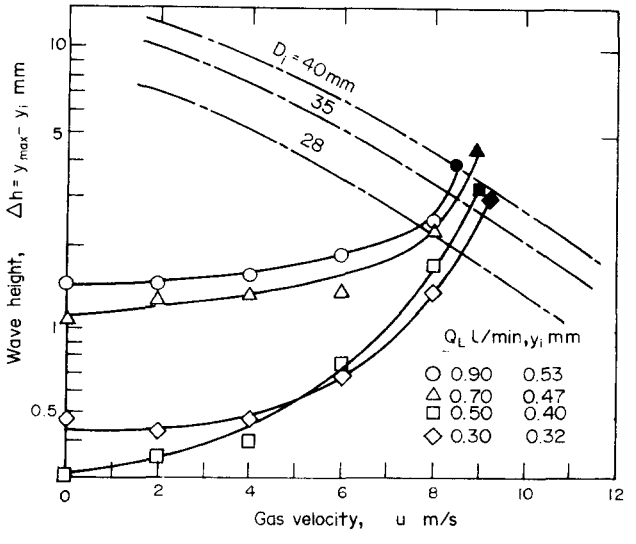

Figure 8. Relation between wave height and gas velocity for air–water flow in an annulus. (D_i = 40 mm, Probe position L = 0.90 m).

experimental results on the annulus of $D_i = 40$ mm shown in figure 6. The wave height increases with increasing gas velocity. The solid points represent the states just before the flooding. As is seen in this figure, the solid points are located close to the corresponding broken line, i.e. the predicted limit condition for $D_i = 40$ mm.

The predicted limit conditions show that as the shroud diameter is reduced, the wave height at the onset of flooding becomes lower and then flooding takes place at a lower gas velocity. The growth of waves on the falling liquid film with increasing upward gas velocity seems to be caused mainly by deceleration of large waves due to the gas stream on the waves and subsequent agglomeration with the following small waves. In fact, it was observed that the wave frequency decreases with increasing wave amplitude. Then, the relation between the wave height and the gas velocity is thought to be approximately independent of the shroud diameter. Therefore, the flooding velocities for the annuli of $D_i = 35$ and 28 mm are predicted as the gas velocities at the intersection points of the measured curves of Δh–u and the predicted limiting curves for $D_i = 35$ and 28 mm in figure 8. The predicted values of flooding velocity are shown in table 2 comparing with the measured values. As is evident from this table, the predicted values are in good agreement with the measured values within $\pm 6\%$.

Next, apply the above analysis to the flow in circular tubes. As an example, figure 9 shows the measured curves of Δh–u for a circular tube of $D_i = 28.8$ mm presented in the previous paper and the predicted limiting curves for flooding condition of various surface tensions. In the calculation of these limiting curves, η_c and y_i are assumed as 1.5 and 0.76 mm, respectively, although the value of y_i has little effect on the curves. It was difficult to measure the wave height Δh just before flooding. However, the flooding velocities can be estimated from intersection points of the extensions of the measured Δh–u curves and the predicted limiting curves as shown in the figure. The predicted values of flooding velocity are compared with the measured results in table 3. The deviation of the predicted values from the measured is within about $\pm 20\%$.

Table 2. Comparison of the predicted flooding velocities with the experimental results (air–water flow in annuli)

Flooding velocity u_G (m/s)		(1): predicted value (2): measured value		
	D_i mm			
Q_L l/min		28	35	40
0.30	(1)	8.53	9.05	9.33
	(2)	8.32	9.05	9.32
0.50	(1)	8.32	8.78	9.08
	(2)	8.00	8.70	9.06
0.70	(1)	7.95	8.45	8.70
	(2)	7.76	8.36	8.97
0.90	(1)	7.72	8.30	8.50
	(2)	7.29	8.19	8.56

Table 3. Comparison of the predicted flooding velocities with the experimental results (flow in a circular tube, $D_i = 28.8$ mm)

Flooding velocity u_G (m/s)		(1): predicted value (2): measured value				Flooding velocity u_G (m/s)		(1): predicted value (2): measured value		Flooding velocity u_G (m/s)		(1): predicted value (2): measured value	
	σ N/m						μ_L Ns/m^2				μ_L Ns/m^2		μ_L Ns/m^2
Q_L l/min		0.068	0.055	0.046	0.037	Q_L l/min	2.1×10^{-3}	Q_L l/min	5.1×10^{-3}	Q_L l/min		Q_L l/min	10×10^{-3}
2	(1)	6.90	7.15	7.42	6.52	1.25	(1) 7.68	0.94	(1) 7.10	0.59	(1) 7.18		
	(2)	7.89	8.24	8.55	7.47		(2) 9.11		(2) 8.85		(2) 9.14		
4	(1)	7.10	6.75	7.35	6.68	2.6	(1) 6.13	2.2	(1) 6.32	1.6	(1) 6.40		
	(2)	5.62	7.55	7.39	6.68		(2) 7.42		(2) 7.41		(2) 6.93		
6	(1)	5.13	6.12	6.35	6.10	5.2	(1) 6.42	4.2	(1) 5.82	3.1	(1) 5.78		
	(2)	3.79	6.90	7.06	5.76		(2) 6.69		(2) 6.31		(2) 5.60		

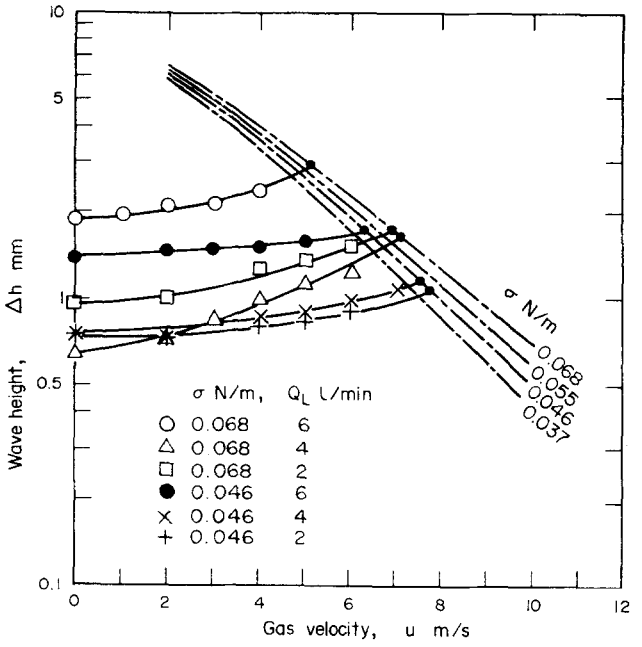

Figure 9. Relation between wave height and gas velocity for flow in a circular tube. (Tube diameter D_i = 28.8 mm, Probe position L = 1.75 m).

Then, as mentioned above, the flooding phenomenon is considered to take place when the force balances in both horizontal and vertical directions are realized on the liquid lump of a large amplitude wave which is developed on the liquid film with an increase of the gas velocity.

5. EXPERIMENTS ON FLOW IN ROD BUNDLES

Figure 10 shows the experimental results of flooding velocity for air–water flow in the bundles of four rods plotted versus the liquid flow rate per rod Q_L and the mean film thickness y_i. The flooding velocity decreases in all cases with increasing the liquid flow rate. Figure 10(a) depicts the results obtained in the case where the rod-rod clearance δ is equal to the rod-shroud clearance δ', (b) is the results of $\delta = 4.1$ mm and (c) is the results of $\delta' = 4.1$ mm. Flooding velocity becomes higher as the clearances δ and δ' are increased.

However, the results for small clearances as 2.3 and 2.5 mm are close to those for the clearance of 4.1 mm. With respect to this, the velocity profile of single-phase air flow was measured across the rod bundles. Figure 11 shows an example of the results obtained at a mean gas velocity of 7.5 m/s. As the clearance is reduced, the velocity variation becomes expectedly large across the rod bundle and the velocity in the narrow section in which the large amplitude wave appears to be initiated becomes lower than the mean gas velocity. It may be attributed to this fact that the flooding velocities at $\delta = \delta' = 2.3$ mm and $\delta' = 2.5$ mm take slightly higher values than those expected from the other data in figure 10.

As a convenient method for describing the effects of the geometry and the cross-sectional area of the channel on the flooding velocity, the following equivalent diameter was introduced,

$$D_{eq} = \frac{4A_s}{\pi(D_i + nd)} \qquad [12]$$

where A_s is the cross-sectional area of the flow passage and n the number of rods supplied liquid. Figure 12 shows the results of flooding velocity in annuli and bundles of three and four rods. It is found from this figure that the flooding velocity shows a general trend to increase with an increase of the equivalent diameter and then the effect of the channel cross-section on

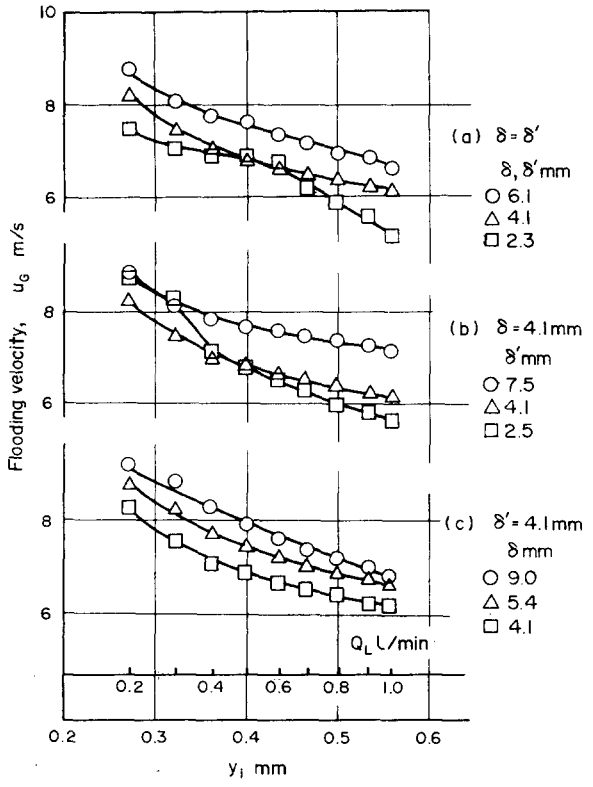

Figure 10. Flooding velocity for air-water flow in bundles of four rods.

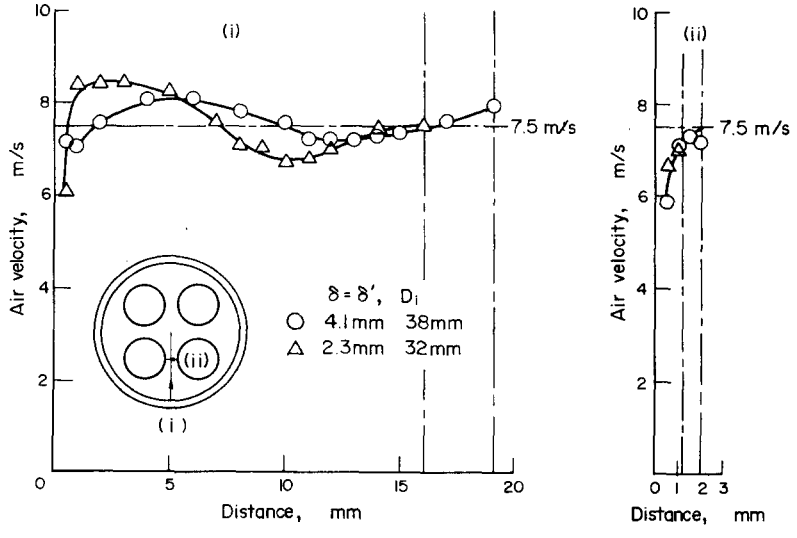

Figure 11. Air velocity profile in bundles of four rods.

flooding appears to be adequately taken into account by using the equivalent diameter. Some experiments were performed by supplying liquid only a part of rods in the bundles. The data of flooding velocity in these experiments were also well correlated by the equivalent diameter defined by[12].

6. EMPIRICAL CORRELATION OF FLOODING VELOCITY

The present data of flooding velocity for flow in annuli and rod bundles are correlated here in the same representation as that for flow in circular tubes; i.e.[8] in Part 1, by applying the equivalent diameter D_{eq} in place of the tube diameter D_i.

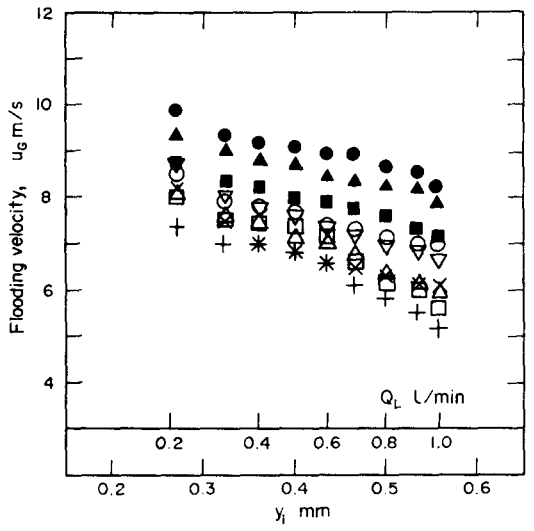

Figure 12. Flooding velocity for air–water flow in annuli and rod bundles of $\delta = \delta'$.

Equivalent diameter D_{eq} (mm)

Annulus	Bundle of four rods	Bundle of three rods
● 30.0	▽ 19.1	○ 18.6
▲ 25.0	× 13.4	△ 14.2
■ 18.0	+ 8.7	□ 8.3

According to the nondimensional representation of flooding velocity for flow in circular tubes, the ordinate was the Froude number

$$Fr = \sqrt{\left(\frac{\rho_G (u_G + u_L)^2}{\rho_L g y_i}\right)} \qquad [13]$$

and the abscissa the nondimensional quantity including a modified surface tension σ',

$$X = \left(\frac{1}{Re_L}\right)^{1/3} \left(\frac{\rho_L g D_{eq}^2}{\sigma'}\right)^{1/4} \left(\frac{\mu_G}{\mu_L}\right)^{2/3}, \qquad [14]$$

$$\sigma' = \sigma + 1.5|\sigma - 0.05| \quad \text{N/m}. \qquad [15]$$

For the channel length $L_d = 1.0$ m, the empirical equation was given by

$$Fr = 8.29 \log_{10} X + 19.18. \qquad [16]$$

Figures 13–15 show the results of flooding velocity in annuli and bundles of four and three rods which are rearranged in the form of [13] and [14]. Equation [16] (solid lines in these figures) is in good agreement with the present results except those of $D_{eq} \leqq 10$ mm. The data plots for $D_{eq} \leqq 10$ mm fall above the solid lines. This discrepancy can be ascribed to the low gas velocities in the narrow section as mentioned before.

7. CONCLUSIONS

(1) Considering the equilibrium state of forces exerted on the liquid lump of a large amplitude wave formed on the liquid film, a limiting condition relating the maximum wave height to the gas velocity at the onset of flooding was derived as [11].

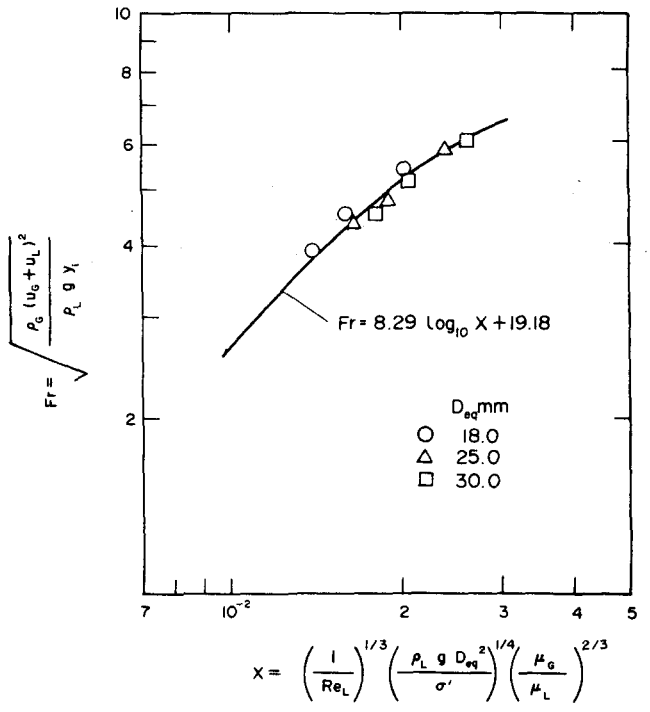

Figure 13. Flooding velocity correlation (annuli).

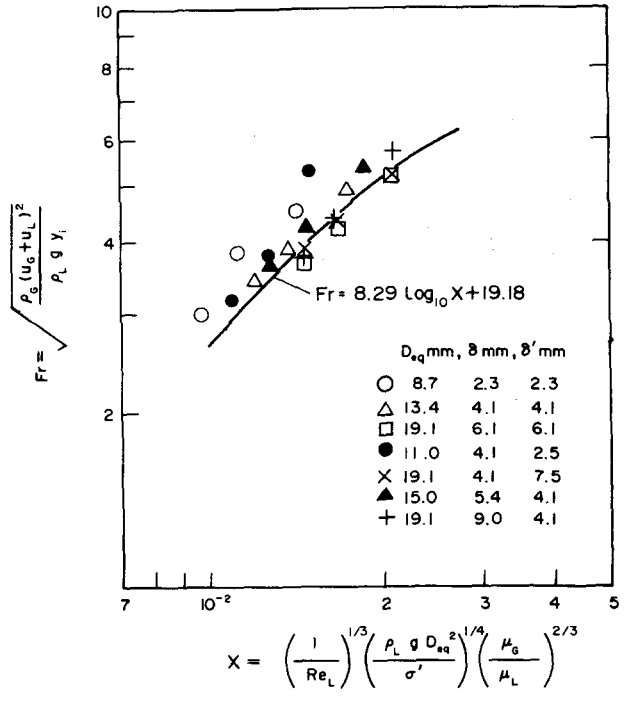

Figure 14. Flooding velocity correlation (bundles of four rods).

(2) The flooding velocity was predicted as the gas velocity at the intersection point of the measured wave height curve for gas velocity and the limit condition of [11]. The predicted values of flooding velocity showed a good agreement with the measured values.

(3) It was found that applying the equivalent diameter of the channel defined as [12], the data

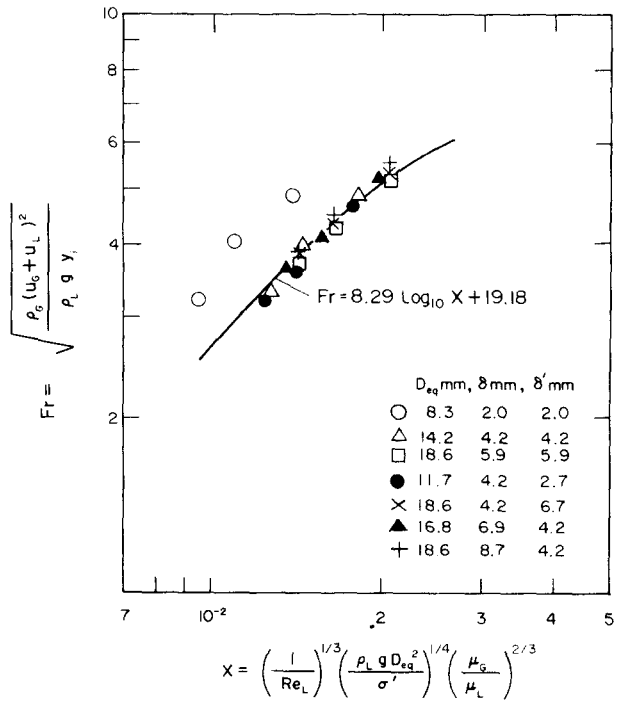

Figure 15. Flooding velocity correlation (bundles of three rods).

of flooding velocity for flow in annuli and rod bundles were well correlated by the same empirical equation as that for flow in circular tubes, if the equivalent diameter was not less than 10 mm.

REFERENCES

GETINBUDAKLER, A. G. & JAMESON, G. J. 1969 The mechanism of flooding in vertical counter-current two-phase flow. *Chem. Engng Sci.* **24**, 1669–1680.

KUSUDA, H. & IMURA, H. 1974 Stability of a liquid film in a counter-current annular two-phase flow. *Trans. Jap. Soc. Mech. Engrs* **40**, 1082–1088.

SHEARER, C. J. & DAVIDSON, J. F. 1965 The investigation of a standing wave due to gas blowing upwards over a liquid film; its relation to flooding in wetted-wall columns. *J. Fluid Mech.* **22**, 321–335.

SHIRES, G. L. & PICKERING, A. R. 1965 The flooding phenomenon in counter-current two-phase flow. *Proc. Symp. on Two-Phase Flow*, Exeter **2**, B501–538.

SHIRES, G. L., PICKERING, A. R. & BLACKER, P. T. 1964 Film cooling of vertical fuel rods. AEEW-R343.

STAINTHORP, F. P. & BATT, R. S. W. 1965 The wave properties of falling liquid films with counter-current air flow. *Proc. Symp. on Two-Phase Flow*, Exeter **2**, B301–310.

SUZUKI, S. & UEDA, T. 1977 Behaviour of liquid films and flooding in counter-current two-phase flow. Part 1, Flow in circular tubes. *Int. J. Multiphase Flow* **3**, 517–532.